Simulation of Quantum Effects in the Nano-scale Semiconductor Device

Seonghoon Jin, Young June Park, and Hong Shick Min

Abstract—**An extension of the density-gradient model to include the non-local transport effect is presented. The governing equations can be derived from the first three moments of the Wigner distribution function with some approximations. A new nonlinear discretization scheme is applied to the model to reduce the discretization error. We also developed a new boundary condition for the Si/SiO$_2$ interface that includes the electron wavefunction penetration into the oxide to obtain more accurate C-V characteristics. We report the simulation results of a 25-nm metal-oxide-semiconductor field-effect transistor (MOSFET) device.**

Index Terms—**MOSFET, Quantum effect, Simulation, Density-gradient model, Hydrodynamic model**

I. INTRODUCTION

As the semiconductor device is scaled down aggressively, its various characteristic lengths are now comparable to the thermal de Broglie wavelength. The electrical characteristics are changed by the emerging quantum effect and the non-local carrier transport significantly. Therefore, semi-classical transport models such as the drift-diffusion (DD) model [1] or the hydrodynamic (HD) model [2] need some modification to include the quantum effect in the simulation of the recent nano-scale devices. There exist quantum transport models that directly calculate the non-equilibrium Green function or the Wigner distribution function and obtain the device characteristics from these functions [3], [4]. But such rigorous quantum transport models cannot be applied to the rather complex multi-dimensional device structure easily. To find out numerically tractable models that can overcome the limits of the semi-classical models, various quantum corrected transport models have been proposed and applied [5]-[16]. Among them, the density-gradient (DG) model extends the DD model by including an effective quantum potential in the drift term and it has become one of the successful models that can simulate the quantum effect [6], [7], [12]-[16]. But the DG model cannot be applied to the highly non-equilibrium condition since it is based on the local equilibrium approximation. Since the inaccuracy of the DG model stems from the inappropriate semi-classical transport model, hydrodynamic extension of the DG model becomes necessary to include the non-local transport effect in addition to the quantum effect.

In Section II, we extend the density-gradient model by including higher order moments of the Wigner distribution function and explain the approximations used in the derivation. We also explain the boundary conditions and related physical parameters of the model in detail. In Section III, we present a new nonlinear discretization scheme that can be used in the unstructured grid. In Secion IV, simulation results of a 25-nm NMOSFET device will be presented followed by conclusions in Section V.

II. BASIC MODELS

A. Derivation

For simplicity, we will derive the equations for electrons only since the equations for holes can be derived similarly. The Wigner distribution function is defined as [5]

Manuscript received JANUARY 12, 2004; revised MARCH 11, 2004.
School of Electrical Engineering and Computer Science, Seoul National University, Seoul 151-744, Korea

$$f\left(\mathbf{k},\mathbf{r},t\right)=\int_{-\infty}^{\infty} d\mathbf{u}\mathbf{r}\left(\mathbf{r}+\frac{\mathbf{u}}{2},\mathbf{r}-\frac{\mathbf{u}}{2},t\right)e^{-i\mathbf{k}\cdot\mathbf{u}}, \quad (1)$$

where

$$\boldsymbol{r}\left(\mathbf{r},\mathbf{r}'\right)=\sum_i p_i \left\langle \mathbf{r} \middle| i \right\rangle \left\langle i \middle| \mathbf{r}' \right\rangle \quad (2)$$

is the density matrix and i labels a complete set of states and p_i are real-valued probabilities for the system to be in the ith state. From the time evolution of the states, the equation of motion for the Wigner distribution function can be written as [4]

$$\frac{\partial f}{\partial t}+\mathbf{v}\cdot\nabla_r f-\sum_{l=0}^{\infty}\frac{\left(-1\right)^l\left(\nabla_r\cdot\nabla_k\right)^{2l+1}Vf}{\hbar 4^l\left(2l+1\right)!}=\left(\frac{\partial f}{\partial t}\right)_C \quad (3)$$

where $V = -q\boldsymbol{y}$ denotes the spatially varying potential energy ($\boldsymbol{y}$ is the electrostatic potential). Note that ∇_k operates only on f and ∇_r operates only on V. The quantum hydrodynamic (QHD) equations can be derived from the moment expansion of (3). The expansion of the equation involves integration of powers of moments (1, $\mathbf{k}$, k^2) against f to obtain conservation laws for the particle, momentum, and energy density. If we assume the steady-state, the isotropic and parabolic band structure, and that the collision term can be approximated by various relaxation times, the resulting conservation equations can be written as [10]

$$\sum_{i=1}^{3}\frac{\partial F_i}{\partial x_i}=0, \quad (4)$$

$$\sum_{j=1}^{3}\frac{\partial}{\partial x_j}\left(\frac{nk_BT_{qij}}{m^*}+\frac{F_iF_j}{n}\right)+\frac{n}{m^*}\frac{\partial V}{\partial x_i}=-\frac{F_i}{\boldsymbol{t}_p}, \quad (5)$$

and

$$\sum_{i=1}^{3}\left(\frac{\partial S_i}{\partial x_i}+\frac{\partial V}{\partial x_i}F_i\right)+n\frac{w-w_0}{\boldsymbol{t}_w}=0, \quad (6)$$

where m^* denotes the effective mass, n is the electron density, $\boldsymbol{t}_p$ and $\boldsymbol{t}_w$ are the momentum and the energy relaxation times,

$$F_i=n\hbar\left\langle k_i\right\rangle/m^* \quad (7)$$

is the i-th component of the carrier flux,

$$T_{qij}=\frac{\hbar^2}{m^*}\left\langle\left(k_i-\left\langle k_i\right\rangle\right)\left(k_j-\left\langle k_j\right\rangle\right)\right\rangle \quad (8)$$

is the temperature tensor,

$$w=\frac{\hbar^2\left\langle k^2\right\rangle}{2m^*} \quad (9)$$

is the average energy, w_0 is the average energy in equilibrium, and

$$S_i=\sum_{j=1}^{3}\left[Q_{ij}+F_i\left(\frac{k_BT_{qjj}}{2}+\frac{m^*F_j^2}{2n^2}\right)+F_jk_BT_{qij}\right] \quad (10)$$

is the energy flux density. In the above equation,

$$Q_{ij}=\frac{\hbar^3 n}{2m^{*2}}\left\langle\left(k_i-\left\langle k_i\right\rangle\right)\left(k_j-\left\langle k_j\right\rangle\right)^2\right\rangle \quad (11)$$

is the heat flux. Note that the forms of (4), (5), and (6) are identical to those of the semi-classical counterparts. To simplify the above equations, we first neglect the drift energy in the energy flux and the convection term in the momentum balance equation. Note that these terms are also neglected in the conventional HD model. Secondly, we must approximate Q_{ij}, w-w_0, and T_{qij} in terms of the scalar electron temperature T. The heat flux is approximated by the Fourier law as

$$\sum_{j=1}^{3}Q_{ij}=-\boldsymbol{k}\frac{\partial T}{\partial x_i} \quad (12)$$

where $\boldsymbol{k}$ is the thermal conductivity. We can also assume that

$$w-w_0=\frac{3}{2}k_B\left(T-T_0\right) \quad (13)$$

where T_0 is the lattice temperature. To approximate T_{qij},

we apply the temperature tensor expression and the relation between n and V valid at the thermal equilibrium as [5]

$$T_{qij} = T\delta_{ij} + \frac{\hbar^2}{12m^* k_B^2 T}\frac{\partial^2 V}{\partial x_i \partial x_j} + O\left(\hbar^4\right), \quad (14)$$

$$V = -k_B T \ln\left(n/C\right) + O\left(\hbar^2\right), \quad (15)$$

and

$$\frac{\partial V}{\partial x_i} = -k_B T \frac{\partial \ln n}{\partial x_i} + O\left(\hbar^2\right) \quad (16)$$

to obtain final expressions up to $\hbar^2$ order. It is noted that $F_i T_{qjk} = F_i T\delta_{jk} + O(\hbar^4)$ since F_i does not contain the zeroth order terms with respect to $\hbar^2$ by (15) and (16). The resulting equations for the carrier flux, energy balance, and energy flux can be written as

$$\mathbf{F} = \mu n \nabla\left(\psi + \psi_q\right) - \mu \nabla\left(\frac{k_B T}{q} n\right), \quad (17)$$

$$\nabla \cdot \mathbf{S} - q\nabla\psi \cdot \mathbf{F} + n\frac{3}{2}k_B \frac{T - T_0}{\tau_w} = 0, \quad (18)$$

and

$$\mathbf{S} = -\kappa \nabla T + \frac{5}{2}k_B T \mathbf{F}, \quad (19)$$

where $\mu = q\tau_p/m^*$ is the mobility and

$$\psi_q = 2b\frac{\nabla^2\sqrt{n}}{\sqrt{n}} \quad (20)$$

is the effective quantum potential and $b = \hbar^2/(12qm^*)$ is the linear gradient coefficient. Note that the quantum correction only appears in the drift term of the carrier flux. The thermal conductivity can be written as

$$\kappa = \left(\frac{5}{2} + c\right)\frac{k_B^2}{q} T\mu n \quad (21)$$

using the Wiedemann-Frantz law.

Since (14), (15), and (16) are valid only at the thermal equilibrium condition, the obtained equations may be invalid at the non-equilibrium condition. However, we believe that applying the equations to non-equilibrium conditions can be a reasonable approximation when the quantum mechanical tunneling is not the main transport mechanism. Therefore, our model is useful when the quantum effect is significant in the perpendicular direction to the direction of the carrier transport (e.g. MOSFET), while it cannot be applied to the simulation of the quantum mechanical devices such as the resonant tunneling diode.

We solve (4), (18), and (20) self-consistently with the Poisson equation

$$-\nabla \cdot \left(\varepsilon \nabla \psi\right) - q\left(p - n + N_D^+ - N_A^-\right) = 0, \quad (22)$$

where ε is the electric permittivity, p is the hole density, and N_D^+ and N_A^- are the ionized donor and acceptor densities. Note that our hydrodynamic density-gradient (HDG) model exactly returns to the conventional HD model in the classical limit ($\psi_q \rightarrow 0$) and the DG model in thermal equilibrium ($T \rightarrow T_0$).

B. Boundary Conditions

There exist three kinds of boundaries in the simulation domain: electrodes, Si/SiO_2 interfaces, and artificial boundaries with the Neumann boundary conditions for fluxes [1]. We only explain the boundary condition for (20) since the boundary conditions for the other equations are equal to the conventional HD model. At the electrodes, the quantum potential ψ_q is assumed to be zero since these regions are usually heavy doped and the electron density becomes uniform.

Special attention should be given to the Si/SiO_2 interfaces. The conventional DG model usually sets vanishingly small electron density at the interface by assuming infinite Si/SiO_2 potential barrier [13]. But this insulating boundary condition overestimates the quantum confinement effect since the actual potential barrier is

finite and the electron wavefunction can penetrate into the oxide. Therefore, we present a new boundary condition by the following assumptions. The electron density penetrated into the oxide by x from the Si/SiO_2 interface can be approximated as [17]

$$n(x) = n(0)\exp(-2x/x_p), \qquad (23)$$

where $n(0)$ is the electron density at the interface and

$$x_p = \frac{\hbar}{\sqrt{2m_{ox}\Phi_B}} \qquad (24)$$

is the characteristic penetration depth obtained from the WKB approximation. Here m_{ox} ($0.5m_0$) and Φ_B (3.15 eV) are the electron effective mass and the potential barrier of the oxide respectively. From (23), the outward normal component of the $b\nabla\sqrt{n}$ at the interface can be written as

$$n \cdot b\nabla\sqrt{n} = -(b_{ox}/x_p)\sqrt{n}, \qquad (25)$$

where $b_{ox} = \hbar^2/(12qm_{ox}^*)$ is the linear gradient coefficient for the oxide region. The value of m_{ox}^* is chosen to be $0.22m_0$ to match the one-dimensional MOS capacitor simulation results obtained by our model and the self-consistent Schrödinger equation solver. With this boundary condition, the electron density at the interface is not a predefined value but an unknown variable. Table I summarizes the boundary conditions of the governing equations.

Table I. Boundary conditions for the governing equations.

Electrode	Interface	Other
$\psi = \psi_0$	$\psi_{Si} = \psi_{SiO_2}$	$\nabla\psi \cdot \mathbf{n} = 0$
$\sqrt{n} = \sqrt{n_0}$	$\mathbf{F} \cdot \mathbf{n} = 0$	$\mathbf{F} \cdot \mathbf{n} = 0$
$\psi_q = 0$	$\mathbf{n} \cdot b\nabla\sqrt{n} = -b_{ox}\sqrt{n}/x_p$	$b\nabla\sqrt{n} \cdot \mathbf{n} = 0$
$T = T_0$	$\mathbf{S} \cdot \mathbf{n} = 0$	$\mathbf{S} \cdot \mathbf{n} = 0$

C. Physical Parameters

The simulation results largely depend on the electron mobility and the energy relaxation time. The low field mobility model should be modified since the previous mobility models assume the classical electron distribution in the MOSFET inversion layer. We modified the Darwish model [18] to fit the universal effective mobility curve when the electron distribution is changed by the quantum effect [19]. Apart from the Darwish model, our model can be applied to the accumulation layer. As for the temperature dependent mobility model, we apply the Caughey-Thomas expression with the effective field approach as [20]

$$\mu(T) = \mu_0\left[1 + \left\{\frac{3k_B\mu_0(T - T_0)}{2qv_{sat}^2\tau_w}\right\}^{\beta}\right]^{-1/\beta}, \qquad (26)$$

where μ_0 is the low field mobility, β=2, and v_{sat} is assumed to be 8×10^6 cm/sec in the inversion layer. The energy relaxation time τ_w is set to be 0.05 psec since the low field mobility of the simulated device is rather small [21].

III. DISCRETIZATION SCHEME

The governing equations are discretized by the conventional control volume method (CVM). In the CVM, the numerical error largely depends on the discretized flux forms in the governing equations. First, let us consider the discretization of **F** and **S**. Except for the additional quantum potential in the drift term of **F**, the functional forms of these fluxes in the model are identical to those in the HD model. Therefore we can adopt the generalized Scharfetter-Gummel (SG) scheme for these equations. The discretized form of F along the mesh line between the adjacent i-th and j-th nodes can be written as [2]

$$F = -D\frac{\Delta T}{\Delta x \ln(T_j/T_i)}\left[B(\tilde{\Delta})\frac{n_j}{T_j} - B(-\tilde{\Delta})\frac{n_i}{T_i}\right], \qquad (27)$$

where n_i, T_i, n_j, and T_j are the electron density and

electron temperature at the i-th and j-th nodes respectively. Also, $\Delta x = x_j - x_i$, $\Delta T = T_j - T_i$, $B(x)$ is the Bernoulli function, and

$$\tilde{\Delta} = \ln\left(\frac{T_j}{T_i}\right)\left[\frac{q\left(\Delta\psi + \Delta\psi_q\right)}{k_B \Delta T} - 2\right]. \tag{28}$$

Similarly, the discretized form of S can be written as

$$S = -\left(\frac{5}{2} + c\right)\frac{k_B D}{\Delta x}\tilde{N}\left[B(\Phi)T_j - B(-\Phi)T_i\right], \tag{29}$$

where

$$\tilde{N} = \frac{\Delta T}{\ln\left(T_j / T_i\right)T_j}\frac{n_j}{}\frac{B(\tilde{\Delta})}{B(\tilde{\Phi})}, \tag{30}$$

$$\tilde{\Phi} = \ln\left(\frac{T_j}{T_i}\right)\left[\frac{q\left(\Delta\psi + \Delta\psi_q\right)}{k_B \Delta T} - 1\right] - \ln\frac{n_j}{n_i}, \tag{31}$$

and

$$\Phi = \frac{5/2}{5/2 + c}\tilde{\Phi}. \tag{32}$$

To obtain the discretized form of $b\nabla\sqrt{n}$, the previous DG model applied the simple central difference scheme by assuming linear dependence of the $\sqrt{n}$ along the mesh line. But this assumption is inconsistent with the generalized SG scheme and it may give rise to large numerical error near the interface and the junction regions where the electron density varies very rapidly. Therefore, we use the functional form of the electron density that can be obtained from the derivation of (27) as

$$n(x) = \frac{n_i}{T_i}T(x)\left[1 - Q(x)\right] + \frac{n_j}{T_j}T(x)Q(x), \tag{33}$$

where

$$T(x) = T_i + \left(\Delta T / \Delta x\right)\left(x - x_i\right) \tag{34}$$

and

$$Q(x) = \frac{\exp\left[\left\{\frac{q(\Delta\psi + \Delta\psi_q)}{k_B \Delta T} - 2\right\}\ln\frac{T(x)}{T_i}\right] - 1}{\exp\left[\left\{\frac{q(\Delta\psi + \Delta\psi_q)}{k_B \Delta T} - 2\right\}\ln\frac{T_j}{T_i}\right] - 1}. \tag{35}$$

Since this functional form is consistent with the generalized SG scheme and it varies exponentially near the interface or the junction by the weighting factor Q(x), it gives more accurate electron density in these cases. From the above expressions, the discretized form of $b\nabla\sqrt{n}$ can be written as

$$b\nabla\sqrt{n} = \frac{b}{2\sqrt{n_{ij}}}\left(\frac{dn}{dx}\right)_{ij}, \tag{36}$$

where

$$n_{ij} = \frac{n_i}{T_i}T_{ij}\left[1 - Q_{ij}\right] + \frac{n_j}{T_j}T_{ij}Q_{ij}, \tag{37}$$

$$\begin{aligned}\left(\frac{dn}{dx}\right)_{ij} &= \frac{\Delta T}{\Delta x}\left[\frac{n_i}{T_i}\left(1 - Q_{ij}\right) + \frac{n_j}{T_j}Q_{ij}\right] \\ &\quad + \left(\frac{dQ}{dx}\right)_{ij}T_{ij}\left(\frac{n_j}{T_j} - \frac{n_i}{T_i}\right),\end{aligned} \tag{38}$$

$$Q_{ij} = \frac{B(\tilde{\Delta})}{B(\tilde{\Lambda})}\frac{\ln\left(T_{ij} / T_i\right) / \Delta T}{\ln\left(T_j / T_i\right) / \Delta T}, \tag{39}$$

$$\left(\frac{dQ}{dx}\right)_{ij} = \frac{B(\tilde{\Delta})}{\Delta x}\frac{\Delta T}{T_{ij}\ln\left(T_j / T_i\right)}\exp\left(\tilde{\Lambda}\right), \tag{40}$$

$$\tilde{\Lambda} = \ln\left(\frac{T_{ij}}{T_i}\right)\left[\frac{q\left(\Delta\psi + \Delta\psi_q\right)}{k_B \Delta T} - 2\right], \tag{41}$$

and

$$T_{ij} = \left(T_i + T_j\right)/2. \tag{42}$$

The obtained expression looks rather complex, but since all the dependant parameters are the local variables at the i-th and j-th nodes, it can be implemented with little loss of efficiency.

If T is uniform and equal to T_0, the above expression for n_{ij} and $\left(\frac{dn}{dx}\right)_{ij}$ can be simplified to

$$n_{ij} = n_i\left(1 - Q_{ij}\right) + n_j Q_{ij} \tag{43}$$

and

$$\left(\frac{dn}{dx}\right)_{ij} = \left(n_j - n_i\right)\left(\frac{dQ}{dx}\right)_{ij}, \tag{44}$$

where

$$Q_{ij} = \frac{1}{1 + \exp\left(\dfrac{\Delta\psi + \Delta\psi_q}{2V_t}\right)} \tag{45}$$

and

$$\left(\frac{dQ}{dx}\right)_{ij} = \frac{B\left(\dfrac{\Delta\psi + \Delta\psi_q}{V_t}\right)}{\Delta x}\exp\left(\frac{\Delta\psi + \Delta\psi_q}{2V_t}\right), \tag{46}$$

where $V_t = k_B T/q$ is the thermal voltage. This expression can be applied to the conventional DG model.

IV. Simulation Results and Discussion

We simulate a bulk NMOSFET whose effective channel length is 25 nm and physical oxide thickness is 1.5 nm [22]. The gate material is uniformly doped (5×10^{20} cm^{-3}) n^+ polysilicon and the channel doping profile is based on the super-halo to prevent the short-channel effect [23]. Fig. 1 shows the doping profile of the device. From this figure, we can find that the source/drain junction depth is 25 nm and the metallurgical channel length is 22 nm.

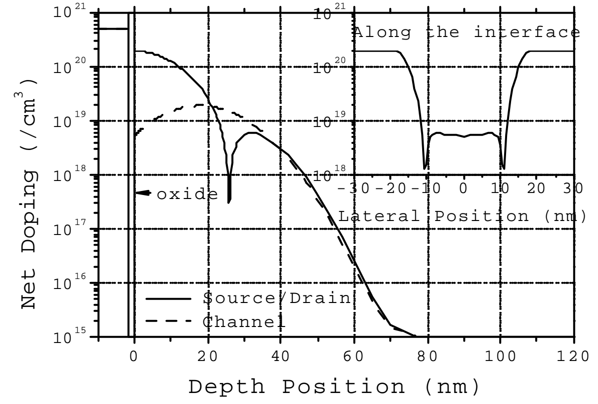

Fig. 1. Doping profile of the 25 nm NMOSFET under consideration

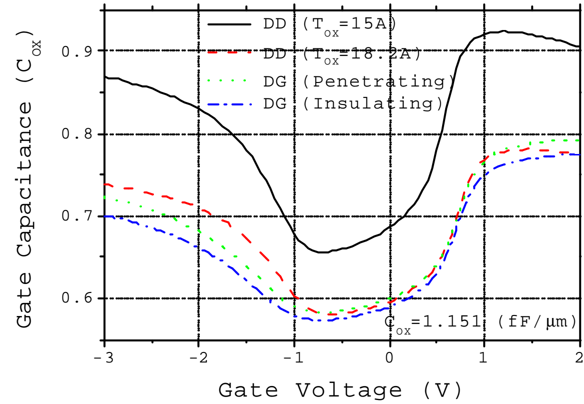

Fig. 2. Comparison of the C_G-V_G characteristics between the DD model t_{ox}=15 Å and t_{ox}=18.2 Å and the DG model (the penetrating boundary condition and the insulating boundary condition).

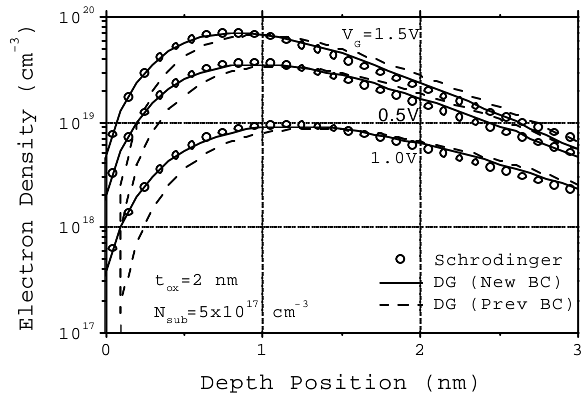

Fig. 3. Comparison of the electron density in the inversion layer between the Schrödinger equation solver, the HDG model with new boundary condition, and the HDG model with old boundary condition.

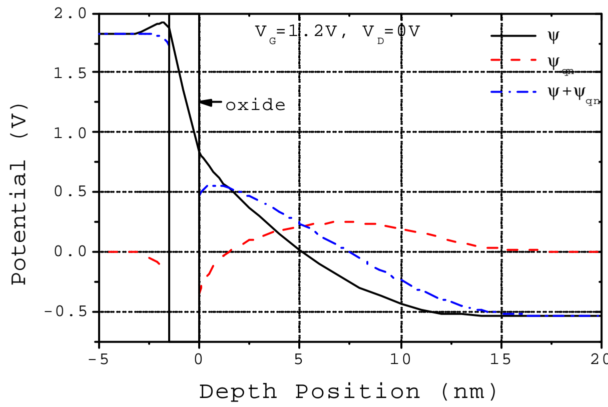

Fig. 4. Comparison of the electrostatic, quantum, and effective potentials along the 1D cut line through the center of the channel.

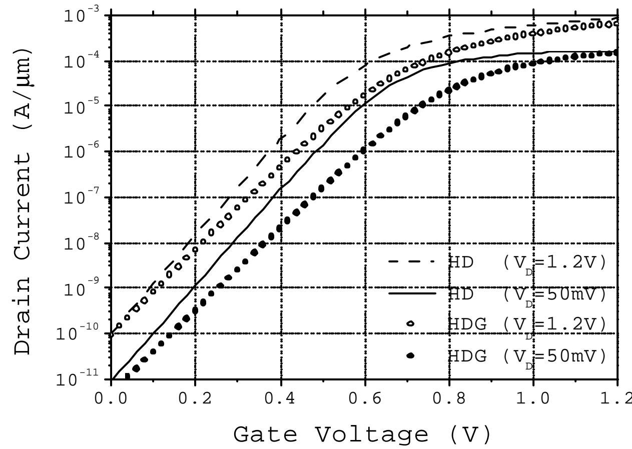

Fig. 5. Comparison of the I_D-V_G characteristics of the MOSFET between the HD and HDG models when V_D is 50 mV and 1.2 V.

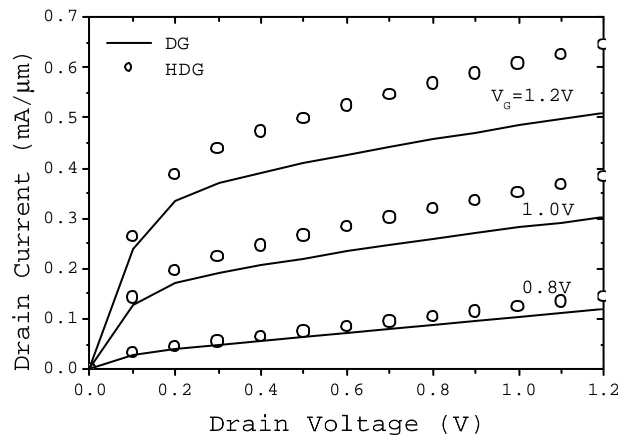

Fig. 6. Comparison of the I_D-V_D characteristics between the DG and HDG models when V_G is 0.8, 1.0, and 1.2V.

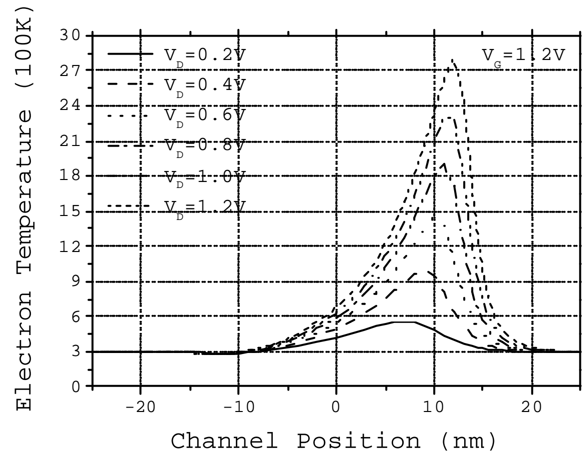

Fig. 7. Electron temperature in the channel when V_G is 1.2 V and V_D is 0.2, 0.4, 0.6, 0.8, 1.0, and 1.2 V.

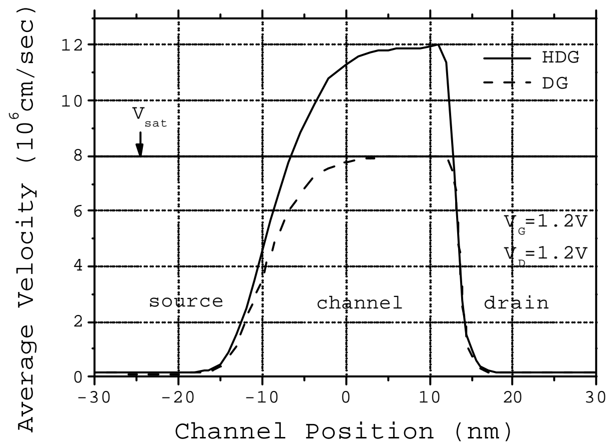

Fig. 8. Comparison of the average electron velocity in the channel between the DG and HDG models when V_G and V_D are 1.2V.

We first study the influence of the quantum effect on the gate capacitance. Fig. 2 shows the C_G-V_G characteristics of the device. The quantum effect reduces the gate capacitance about 20% and increases the effective oxide thickness about 3.2 Å. The interface boundary condition also changes the gate capacitance. The penetrating boundary condition increases the gate capacitance slightly compared with the insulating boundary condition. To see the influence of the interface boundary condition, we plot the electron density in the inversion layer in Fig. 3. As a reference, we calculate the electron density using the self-consistent Schrödinger equation solver. The electron density calculated from the penetrating boundary condition follows the Schrödinger

equation solver very well, while the insulating boundary condition shifts the electron density away from the interface about 1 Å. Fig. 4 shows the electrostatic, quantum, and effective potentials along the 1D cut line through the center of the channel. The quantum potential smoothes the potential variation near the Si/SiO_2 interface, which prevents the electron density vary discontinuously at the interface.

In Fig. 5, we compare the I_D-V_G characteristics between the HD and HDG models. As we include the quantum effect, the subthreshold slope (SS) and drain-induced barrier lowering (DIBL) are increased from 93 mV/dec to 108 mV/dec and from 99 mV to 145 mV respectively. Since the quantum confinement effect increases the effective oxide thickness, the gate electrode cannot control the channel charge effectively, which results in the degradation of the SS and DIBL.

Fig. 6 shows the I_D-V_D characteristics calculated from the DG and HDG models. The HDG model predicts higher on-current up to 26%, which can be explained by the non-local transport effect. Fig. 7 shows the electron temperature in the channel when the bias conditions are in the linear and saturation regions. The electron temperature does not change appreciably until the channel position is about –10 nm, which means that the mobility at the source side of the channel remains high. Fig. 8 shows the average electron velocity in the channel calculated from the DG and HDG models. The HDG model predicts larger electron velocity in the channel, which results in larger on-current. The figure also shows the velocity overshoot effect in the drain side of the channel.

V. CONCLUSION

We obtained the HDG model from the quantum moment equations. The obtained equations are similar to the conventional HD model except for the quantum potential term. Our model can be viewed as a hydrodynamic extension of the DG model and it returns to the HD model in the classical limit and the DG model in thermal equilibrium. We introduced the nonlinear discretization scheme that can reduce the discretization error and improved the boundary condition for the Si/SiO_2 interface by including penetration of wavefunction into the oxide. We applied our model to the 25 nm NMOSFET device, which is close to the limit of the bulk MOSFET. The simulation results show that the quantum effect and the non-local transport effect can change the device characteristics about 20-30 %.

ACKNOWLEDGMENT

The authors appreciate the support of the *National Research Laboratory Project of the Ministry of Science and Technology* and the *Brain Korea 21 Project*.

REFERENCES

[1] S. Selberherr, *Analysis and Simulation of Semiconductor Devices*, Wien, Austria: Springer-Verlag, 1984.
[2] W. S. Choi, J. G. Ahn, Y. J. Park, H. S. Min, and C. G. Hwang, *IEEE Trans. on CAD*, vol. 13, no. 7, pp. 899-908, July 1994.
[3] R. Lake, G. Klimeck, R. C. Bowen, and D. Jovanovic, J. Appl. Phys., vol. 81, no. 12, pp. 7845-7869, June 1997.
[4] W. R. Frensley, Rev. Mod. Phys., vol. 62, no. 3, pp. 745-791, July 1990.
[5] E. Wigner, Phys. Rev., vol. 40, pp. 749-759, June 1932.
[6] M. G. Ancona and H. F. Tiersten, Phys. Rev. B, vol. 35, no. 15, pp. 7959-7965, May 1987.
[7] M. G. Ancona and G. J. Iafrate, Phys. Rev. B, vol. 39, no. 13, pp. 9536-9540, May 1989.
[8] J.-R. Zhou and D. K. Ferry, *IEEE Trans. on ED*, vol. 39, no. 3, pp. 473-478, March 1992.
[9] H. L. Grubin, T. R. Govindan, and J. P. Kreskovsky, *Solid-State Electronics*, vol. 36, no. 12, pp. 1697-1709, 1993
[10] C. L. Gardner, *SIAM Journal on Applied Mathematics*, vol. 54, no. 2, pp. 409-427, April 1994.
[11] D. K. Ferry, R. Akis, and D. Vasileska, *Proc. of IEDM*, pp. 287-290, December 2000.
[12] M. G. Ancona, Z. Yu, R. W. Dutton, P. J. V. Voorde, M. Cao, and D. Vook, *IEEE Trans. on ED*, vol. 47, no. 12, pp. 2310-2319, December 2000.
[13] Z. Yu, R. W. Dutton, and D. W. Yergeau, *Proc. of SISPAD*, pp. 1-9, September 2001.
[14] D. Connelly, Z. Yu, and D. W. Yergeau, *IEEE Trans. on ED*, vol. 49, no. 4, pp. 619-626, April 2002.
[15] E. Lyumkis, R. Mickevicius, O. Penzin, B. Polsky, K. El

Sayed, A. Wettstein, and W. Fichtner, *Proc. of SISPAD*, pp. 271-274, September 2002.
[16] J. R. Watling, A. R. Brown, A. Asenov, A. Svizhenko, and M. P. Anantram, *Proc. of SISPAD*, pp. 267-270, September 2002.
[17] S. Jin, Y. J. Park, and H. S. Min, *Proc. of SISPAD*, pp. 263-266, September 2003.
[18] M. N. Darwish, J. L. Lentz, M. R. Pinto, P. M. Zeitzoff, T. J. Krutsick, H. H. Vuong, *IEEE Trans. on ED*, vol. 44, no. 9, pp. 1529-1538, September 1997.
[19] H. Shin, J. Y. Lee, J.-S. Park, S. Jin, Y. J. Park, and H. S. Min, submitted to *IEEE Trans. on ED*.
[20] *MEDICI User's Manual*, Avant! Corp., Feb. 2001.
[21] G. Baccarani and M. Wordeman, *Solid-State Electronics*, vol. 28, no. 4, pp. 407-416, 1985.
[22] D. A. Antoniadis, I. J. Djomehri, K. M. Jackson, and S. Miller, *Well-Tempered Bulk-Si NMOSFET Device Home Page*, http://www-mtl.mit.edu/Well/, Microsystems Technology Laboratory, MIT.
[23] Y. Taur, C. H. Wann, and D. J. Frank, *Proc. of IEDM*, pp. 789-792, December 1998.

Seonghoon Jin received the B.S. degree in electrical engineering from Seoul National University, Seoul, Korea, in 2001 where he is currently working toward the Ph.D. degree in electrical engineering. His research interests include semiconductor device simulation, quantum transport theory, and reliability and noise modeling in semiconductor devices.

Young June Park received the B.S. and M.S. degrees from Seoul National University, Seoul, Korea in 1975 and 1977, respectively, and the Ph.D. degree from the University of Massachusetts, Amherst, in 1983. From 1983 to 1985, he worked for the Device Physics and Technology Department, IBM, East Fishkill, NY. In 1985, he joined Gold Star Semiconductor Company, Anyang, Kyungki, (currently Hynix Semiconductor Inc.) to work in the area of the CMOS technology. In 1993, he spent his sabbatical year at Stanford University, Stanford, CA, and performed research on advance semiconductor transport model. Since 1988, he has been with Seoul National University (SNU), where he is a Professor in the School of Electrical Engineering and Computer Science. From 1996 to 2001, he served the Inter-University Semiconductor Research Center (ISRC), SNU, as a Director. In 2001, he was on a leave of absence to work for Hynix Semiconductor Inc. as a Director of the Memory Research and Development Division. His areas of interest are the advanced device structures, device/noise and reliability modeling, and low-power circuit technology.

Hong Shick Min received the B.S. degree in electronics engineering from Seoul National University, Seoul, Korea, in 1966, and M.S. and Ph.D. degrees in electrical engineering from the University of Minnesota, Minneapolis, in 1969 and 1971, respectively. From 1971 to 1972, he was a Postdoctoral Fellow at the University of Minnesota. In 1973, he joined the Department of Electronics Engineering at Korea University, Seoul, as an Assistant Professor. Since 1976, he has been with the School of Electrical Engineering, Seoul National University, where he is currently a Professor. His main research interests include noise in semiconductors and semiconductor devices.